Control of atomic dynamics in laser-assisted electron-atom scattering through the driving-laser ellipticity

A. V. Flegel, M. V. Frolov, N. L. Manakov, Anthony F. Starace, and A. N. Zheltukhin

Phys. Rev. A **87**, 033414 — Published 20 March 2013

DOI: 10.1103/PhysRevA.87.033414

Control of Atomic Dynamics in Laser-Assisted Electron-Atom Scattering Through the Driving Laser Ellipticity

A. V. Flegel,[1,2] M. V. Frolov,[3] N. L. Manakov,[3] Anthony F. Starace,[1] and A. N. Zheltukhin[1]

[1] *Department of Physics and Astronomy, The University of Nebraska, Lincoln, NE 68588-0299*
[2] *Department of Computer Science, Voronezh State University, Voronezh 394006, Russia*
[3] *Department of Physics, Voronezh State University, Voronezh 394006, Russia*

(Dated: February 11, 2013)

Orders of magnitude increases of the cross sections are predicted for laser-assisted low-energy electron-atom scattering (accompanied by absorption of laser photons) as the laser ellipticity is increased. These ellipticity-controlled enhancements are manifestations of the field-free electron-atom scattering dynamics, such as the Ramsauer-Townsend effect in low-energy elastic electron-atom scattering. The strong sensitivity of laser-assisted scattering cross sections to this dynamics and the laser ellipticity is illustrated for e-Ne and e-Ar scattering in both mid-infrared ($\lambda = 3.5$ μm) and CO_2 ($\lambda = 10.6$ μm) laser fields of moderate intensities.

PACS numbers: 34.80.Qb, 34.50.Rk, 03.65.Nk

I. INTRODUCTION

The spectra of processes involving intense laser interactions with atoms and molecules typically involve plateau features, i.e., nearly constant cross sections versus the number n of absorbed laser photons over a wide interval of n. These plateaus have been investigated for over two decades in laser-induced above-threshold ionization (ATI) and high-order harmonic generation (HHG) processes [1–3]. The occurrence of plateaus in laser-assisted electron scattering (LAES) was predicted in Ref. [4] (cf. also Ref. [5]), in which it was shown that the LAES spectrum is characterized by two plateaus, related to two different regions of the scattered electron energy. A low-energy plateau is due to "direct" scattering and can be described by the Kroll-Watson (KW) result [6] for the differential cross section (DCS) of LAES in the low-frequency approximation. A second, high-energy plateau was explained [4] similarly to the rescattering scenario for ATI and HHG processes [7, 8]: the laser field drives the scattered electron back to the atom, whereupon the electron gains additional energy from the laser field during the rescattering. Although the occurrence of the high-energy (rescattering) plateaus originates from laser-driven electron motion in the continuum and is not dependent on the internal atomic dynamics, the shape of the plateaus is highly sensitive to this dynamics. Moreover, it was shown numerically [9] and derived analytically [10, 11] that HHG and ATI yields in the region of the rescattering plateau cutoff can be factorized as the product of laser-induced factors and field-free atomic parameters. Recently these factorized results were used to image atomic [12] and molecular [13] structures. An analytic factorized formula for the DCS of LAES in a linearly-polarized laser field was obtained recently using time-dependent effective range (TDER) theory [14].

All the aforementioned studies were for the case of linearly polarized laser fields, whereas only recently has the use of the laser ellipticity been explored as a means to control and provide a deeper understanding of the HHG process [15–19]. In contrast to ATI or HHG, however, rescattering effects in LAES do not disappear with increasing ellipticity. In particular, a rescattering plateau has been predicted for LAES even for circular polarization [20, 21]. Nevertheless, the use of the laser ellipticity to illuminate the influence of field-free electron-atom dynamics on LAES spectra has not yet been investigated.

In this paper we show that the manifestations of field-free electron-atom dynamics in LAES can be controlled by the laser ellipticity. Our study is based on the generalization of our recent TDER results for LAES in an elliptically polarized laser field [22] to the case of electron scattering by neutral atoms. Our results for e-Ne and e-Ar scattering exhibit the high sensitivity of LAES spectra to the target atom, resulting in enhancement of the cross sections for e-Ar scattering by orders of magnitude with increasing laser ellipticity. We show that this latter enhancement originates from the Ramsauer-Townsend (RT) effect [23] in low-energy electron scattering by Ar atoms.

II. ANALYTIC RESULTS FOR THE LAES AMPLITUDE AND CROSS SECTION

We consider the scattering of an electron with momentum $\mathbf{p}$ and energy $E = p^2/(2m)$ by a target atom in a laser field with intensity I and frequency ω assuming that both the electron energy E and the laser photon energy $\hbar\omega$ are small compared to atomic excitation energies and that laser excitation or ionization of atomic electrons is negligible. Under these assumptions, the electron-atom interaction can be approximated by a short-range potential $U(r)$. Thus, the LAES process can be described as potential (elastic) electron scattering accompanied by absorption or emission of n laser photons ($n_{\min} = -[E/(\hbar\omega)]$, where $[x]$ is the integer part of x), so that the momentum (or energy) spectra of scattered electrons (the LAES spectra) are characterized by the

momentum $\mathbf{p}_n$, where $p_n = \sqrt{2m(E + n\hbar\omega)}$.

The electron-laser interaction in the electric dipole approximation is given by $V(\mathbf{r}, t) = -e\mathbf{r}\cdot\mathbf{F}(t)$, where $\mathbf{F}(t)$ is the laser electric field vector, $\mathbf{F}(t) = F\mathrm{Re}\big(\mathbf{e}e^{-i\omega t}\big)$. The complex polarization vector $\mathbf{e}$ is parameterized as

$$\mathbf{e} = (\hat{\boldsymbol{\epsilon}} + i\eta[\hat{\boldsymbol{\kappa}} \times \hat{\boldsymbol{\epsilon}}])/\sqrt{1+\eta^2}, \quad -1 \le \eta \le 1, \qquad (1)$$

where $\hat{\boldsymbol{\epsilon}}$ is a unit vector along the major axis of the polarization ellipse, the vector $\hat{\boldsymbol{\kappa}}$ defines the laser propagation direction, η is the laser ellipticity, and $\mathbf{e}\cdot\mathbf{e}^* = 1$. With the definition (1), the laser intensity does not depend on η: $I = cF^2/(8\pi)$.

For a non-perturbative treatment of both the electron-laser and electron-atom interactions, in Refs. [14, 22] we employed the TDER theory [24], which extends effective range theory [23] for low-energy electron scattering to the case of LAES. The main approximation in the TDER theory is the same as in effective range theory: the interaction of the incident electron with the atomic potential $U(r)$ is taken into account in only a single (e.g., s-wave) continuum channel by means of the scattering phase $\delta_0(E)$, which is parametrized in terms of the scattering length and the effective range. The advantage of TDER theory is that the exact TDER equations for the scattering state of an electron in the field $\mathbf{F}(t)$ can be solved analytically in the limit of a low-frequency field, providing closed-form expressions for the amplitude, $\mathcal{A}_n(\mathbf{p}, \mathbf{p}_n)$, and the DCS for n-photon LAES,

$$d\sigma_n(\mathbf{p}, \mathbf{p}_n)/d\Omega_{\mathbf{p}_n} = (p_n/p)|\mathcal{A}_n(\mathbf{p}, \mathbf{p}_n)|^2. \qquad (2)$$

The final TDER result for $\mathcal{A}_n$ can be presented as a sum of the KW-approximation amplitude, $\mathcal{A}_n^{(\mathrm{KW})}$, and the rescattering amplitude, $\mathcal{A}^{(\mathrm{R})}$: $\mathcal{A}_n = \mathcal{A}_n^{(\mathrm{KW})} + \mathcal{A}_n^{(\mathrm{R})}$.

The KW-approximation amplitude $\mathcal{A}_n^{(\mathrm{KW})}$ in a low-frequency field $\mathbf{F}(t)$ and its comparison with results for $\eta \neq 0$ [25, 26] are discussed in detail in Ref. [22]. For a general scattering geometry this amplitude contains a Bessel function of the first kind, $J_n(x)$, and its derivative, while for forward scattering along the major axis of the polarization ellipse ($\mathbf{p}_n \| \mathbf{p} \| \hat{\boldsymbol{\epsilon}}$) it has the same form as the KW result for $\eta = 0$ [6]:

$$\mathcal{A}_n^{(\mathrm{KW})} = \mathrm{i}^n \mathrm{e}^{in\chi} \mathcal{A}_{el}[\mathbf{P}(t_c), \mathbf{P}_n(t_c)] J_n(\rho), \qquad (3)$$

$$\frac{d\sigma_n^{(\mathrm{KW})}(\mathbf{p}, \mathbf{p}_n)}{d\Omega_{\mathbf{p}_n}} = \frac{p_n}{p} \frac{d\sigma_{el}[\mathbf{P}(t_c), \mathbf{P}_n(t_c)]}{d\Omega_{\mathbf{P}_n(t_c)}} J_n^2(\rho), \qquad (4)$$

where ρ and χ are related to the complex scalar product $\mathbf{e}\cdot\boldsymbol{\Delta}_{\mathbf{p}}$ of the polarization vector $\mathbf{e}$ and the momentum transfer, $\boldsymbol{\Delta}_{\mathbf{p}} = \mathbf{p}_n - \mathbf{p}$:

$$\rho = (\alpha_0/\hbar)|\mathbf{e}\cdot\boldsymbol{\Delta}_{\mathbf{p}}|, \quad \chi = \arg(\mathbf{e}\cdot\boldsymbol{\Delta}_{\mathbf{p}}),$$

where $\alpha_0 = |e|F/(m\omega^2)$ is the classical quiver radius for an electron in the field $\mathbf{F}(t)$. The field-free elastic scattering amplitude, $\mathcal{A}_{el}$, and the DCS, $d\sigma_{el}/d\Omega_{\mathbf{P}_n(t_c)}$, are evaluated at instantaneous laser-modified momenta,

$$\mathbf{P}(t_c) = \mathbf{p} - (e/c)\mathbf{A}(t_c), \quad \mathbf{P}_n(t_c) = \mathbf{p}_n - (e/c)\mathbf{A}(t_c),$$

where $\mathbf{A}(t)$ is the vector-potential of $\mathbf{F}(t)$. The equation for the moment t_c of elastic electron-atom collision is given by the energy conservation law at $t = t_c$: $\mathbf{P}^2(t_c)/(2m) = \mathbf{P}_n^2(t_c)/(2m)$. The amplitude (3) loses its accuracy in the classically-forbidden region of the LAES spectrum (i.e., for $|n| > n_{\max} = [\rho]$), where the time t_c becomes complex. In this region, we approximate $\mathcal{A}_{el}$ by its value at the boundary of the classically-allowed region, $|n| = n_{\max}$, and we note that the amplitude $\mathcal{A}_n^{(\mathrm{KW})}$ decreases exponentially.

The rescattering amplitude $\mathcal{A}_n^{(\mathrm{R})}$ for any scattering geometry is given by a sum of products of three factors, two of which are field-free amplitudes $\mathcal{A}_{el}$ [22]:

$$\mathcal{A}_n^{(\mathrm{R})} = \frac{1}{\alpha_0} \sum_s \mathcal{A}_{el}[\mathbf{P}(t_s), \mathbf{Q}(t_s, t_s')]\, D(t_s, t_s') \times \mathcal{A}_{el}[\mathbf{Q}(t_s', t_s), \mathbf{P}_n(t_s')], \qquad (5)$$

where $\mathbf{Q}(t, t') = (e/c)\left[(t'-t)^{-1}\int_t^{t'} \mathbf{A}(\tau)d\tau - \mathbf{A}(t)\right]$ and the summation is taken over the set of closed classical electron trajectories in the field $\mathbf{F}(t)$. The sth trajectory starts at the time $t = t_s$ of the first collision, accompanied by a change of the electron kinetic momentum from $\mathbf{P}(t_s)$ to the laser-induced momentum $\mathbf{Q}(t_s, t_s')$ (with $|\mathbf{P}(t_s)| = |\mathbf{Q}(t_s, t_s')|$), where the time t_s' of the second collision (rescattering) ensures the return of the electron to the atom over the period $T_s = t_s' - t_s$ with maximum classical energy, $\mathbf{Q}^2(t_s', t_s)/(2m)$, gained by the electron from the laser field at the time t_s'.

The factors $D(t_s, t_s')$ in Eq. (5) are propagation amplitudes describing laser-driven motion of the electron between the collision at $t = t_s$ and recollision at $t = t_s'$:

$$D(t_s, t_s') = \left(\frac{\hbar\omega}{u_p\alpha_s}\right)^{1/3} \frac{\mathrm{e}^{\mathrm{i}\phi_s}\mathrm{Ai}[\zeta(t_s, t_s')]}{\sqrt{\omega^3 T_s^3 \beta_s}}, \qquad (6)$$

$$\zeta(t_s, t_s') = \frac{\mathbf{P}_n^2(t_s') - \mathbf{Q}^2(t_s', t_s)}{2mu_p[(\hbar\omega/u_p)^2\alpha_s]^{1/3}}, \qquad (7)$$

where $\mathrm{Ai}(\zeta)$ is an Airy function, $u_p = e^2F^2/(4m\omega^2)$ is the classical quiver energy, and the dimensionless parameters α_s, β_s and the phase ϕ_s can be expressed in terms of the instantaneous fields $\mathbf{F}(t_s)$, $\mathbf{F}(t_s')$ and momenta $\mathbf{P}(t_s)$, $\mathbf{P}_n(t_s')$ [22]. Since the Airy function in $D(t_s, t_s')$ oscillates for $\zeta(t_s, t_s') < \zeta_0 = -1.019$ and decreases exponentially for $\zeta(t_s, t_s') > \zeta_0$, the sth term in Eq. (5) becomes negligibly small for $\mathbf{P}_n^2(t_s') > \mathbf{Q}^2(t_s', t_s)$ [cf. Eqs. (6) and (7)].

The rescattering plateau cutoff at $n = n_{\max}^{(\mathrm{R})}$ corresponds to the maximum classical energy, $\mathbf{Q}^2(\tau', \tau)/(2m)$, where τ and τ' are the times t_s and t_s' for the shortest closed trajectory, and $n_{\max}^{(\mathrm{R})}$ is a solution of the equation $\zeta(\tau, \tau') = \zeta_0$. Near the rescattering plateau cutoff, only a single term in Eq. (5) (with $t_s = \tau$ and $t_s' = \tau'$) contributes to the LAES amplitude, giving a factorized result for the LAES cross section with absorption of n photons:

$$\frac{d\sigma_n^{(\mathrm{R})}(\mathbf{p}, \mathbf{p}_n)}{d\Omega_{\mathbf{p}_n}} = \frac{d\sigma_{el}(\mathbf{P}, \mathbf{Q})}{d\Omega_{\mathbf{Q}}} W(\mathbf{p}, \mathbf{p}_n) \frac{d\sigma_{el}(\mathbf{Q}', \mathbf{P}_n)}{d\Omega_{\mathbf{P}_n}}, \qquad (8)$$

$$W(\mathbf{p}, \mathbf{p}_n) = p_n/(p\,\alpha_0^2)\,|D(\tau, \tau')|^2. \qquad (9)$$

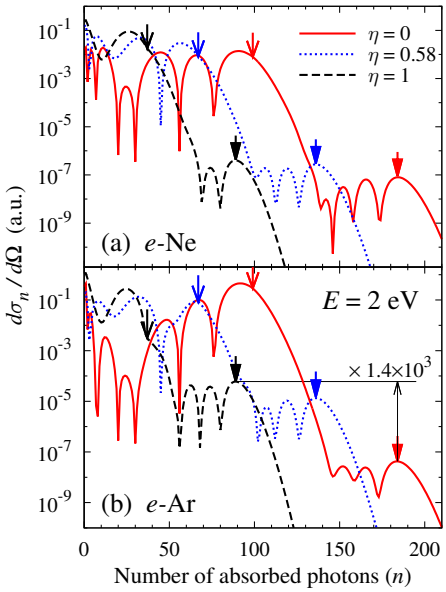

FIG. 1. (Color online) LAES spectra for e-Ne and e-Ar forward scattering ($\mathbf{p}_n \| \mathbf{p} \| \hat{\boldsymbol{\epsilon}}$) in a laser field with $\hbar\omega = 0.354$ eV ($\lambda = 3.5$ μm), $I = 6.2 \times 10^{12}$ W/cm^2 ($u_p = 7.06$ eV) for electron energy $E = 2$ eV, and ellipticities $\eta = 0, 0.58, 1$. The boundaries $n_{\max}$ of the classically-allowed regions of the low-energy plateaus and the cutoffs $n_{\max}^{(\mathrm{R})}$ of the high-energy (rescattering) plateaus are indicated by the unfilled and filled arrows respectively.

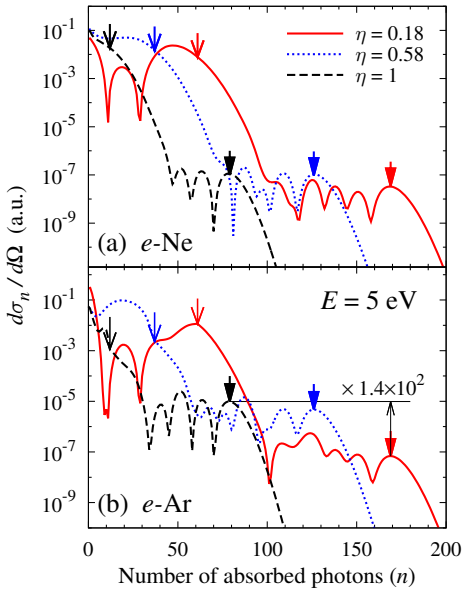

FIG. 2. (Color online) The same as in Fig. 1, but for $E = 5$ eV and $\eta = 0.18, 0.58, 1$.

Owing to its quantum derivation, Eq. (8) gives a quantum expression for the classical three-step scenario for LAES with $\eta \neq 0$. The DCS $d\sigma_{el}(\mathbf{P}, \mathbf{Q})/d\Omega_{\mathbf{Q}}$, with instantaneous kinetic momenta $\mathbf{P} = \mathbf{P}(\tau)$ and $\mathbf{Q} = \mathbf{Q}(\tau, \tau')$, describes elastic scattering at the time τ. The propagation factor $W(\mathbf{p}, \mathbf{p}_n)$ describes the laser-driven motion of the electron over the period $T = \tau' - \tau$ and gives the oscillatory interference pattern of LAES spectra in the high-energy plateau region [14, 22] (cf. also Figs. 1 and 2). The rescattering at time τ' is described by $d\sigma_{el}(\mathbf{Q}', \mathbf{P}_n)/d\Omega_{\mathbf{P}_n}$, where $\mathbf{Q}' = \mathbf{Q}(\tau', \tau)$ and $\mathbf{P}_n = \mathbf{P}_n(\tau')$. Our numerical analysis shows that the result (8) agrees well with exact TDER results in the plateau cutoff region, while the amplitude (5) provides a quantitative description of the entire rescattering plateau [22].

Since the factors $D(t_s, t_s')$ in Eq. (5) [as well as $D(\tau, \tau')$ in Eq. (9)] do not depend on any parameters of the potential $U(r)$, all information about atomic dynamics in LAES is contained entirely in the elastic scattering amplitudes $\mathcal{A}_{el}$, which in the TDER theory are considered in the effective range approximation (cf. Ref. [22]). Thus, in a way similar to the generalization of factorized TDER results for HHG and ATI to the case of neutral atoms [10, 11] (which provide results in excellent agreement with results of numerical solutions of the time-dependent Schrödinger equation), it is reasonable to generalize the analytic formulas (5) and (8) beyond the TDER theory, by replacing the effective range results for $\mathcal{A}_{el}$ and $d\sigma_{el}/d\Omega$ (involving only a single phase shift) by their counterparts for real atoms [involving a full set of phase shifts $\delta_l(E)$]. The latter may be taken from either experiments or precise theoretical calculations. In what follows, we analyze the manifestation of atomic dynamics in LAES spectra of Ne and Ar, using phase shifts $\delta_l(E)$ obtained by a B-spline R-matrix method [27] for electron scattering by Ne and Ar [28].

III. FEATURES OF ATOMIC DYNAMICS IN LAES SPECTRA

In Figs. 1 and 2 we compare LAES spectra [obtained using Eqs. (3) and (5)] for e-Ne and e-Ar scattering for the particular geometry of forward scattering along the major axis of the polarization ellipse, i.e. for $\mathbf{p}_n \| \mathbf{p} \| \hat{\boldsymbol{\epsilon}}$. A very pronounced modification of the shape of the LAES spectrum with variation of the ellipticity for e-Ar scattering in contrast to that for e-Ne scattering illustrates the main result of our study. This modification appears differently in the low-energy and high-energy plateau regions, and is due to the high sensitivity of LAES spectra to details of electron-atom dynamics, i.e., to the dependence of the amplitudes $\mathcal{A}_{el}$ in Eqs. (3) and (5) on the laser-modified momenta, which in turn depend on the laser ellipticity η.

A. The low-energy plateau

The low-energy part of each LAES spectrum in Figs. 1 and 2 is described by the KW cross section (4), which involves only a single atomic factor $d\sigma_{el}/d\Omega$. This factor varies slowly with n and modulates the oscillatory behavior of $d\sigma_n/d\Omega$ (over the classically-allowed region

$|n| < n_{\max}$) stemming from the Bessel function $J_n(\rho)$ in Eq. (4). Numerical results for the collision time $t_c = t_c(\eta, \mathbf{p}, \mathbf{p}_n)$ show that the electron kinetic energy at the moment of collision, $\mathcal{E}(t_c) = \mathbf{P}^2(t_c)/(2m)$, depends significantly on the ellipticity: for $\eta = 0$, $\mathcal{E}(t_c) = 0$ for $n = 0$ and increases with increasing n [e.g., for parameters as in Fig. 1, $\mathcal{E}(t_c)$ increases from zero at $n = 0$ to 5.5 eV at $n = n_{\max} = 99$]; in contrast, for $|\eta| > 0$, $\mathcal{E}(t_c)$ is non-zero for any n.

A pronounced (up to an order of magnitude) suppression of the e-Ar LAES DCS in the low-energy plateau region for $\eta = 0$ in Fig. 1(b) as compared to the relatively constant one for e-Ne scattering in Fig. 1(a) is a manifestation of the well-known Ramsauer-Townsend (RT) effect [23] in the LAES spectrum for e-Ar scattering. Specifically, whereas for Ne the oscillatory maxima of the $\eta = 0$ curve in Fig. 1(a) are approximately constant (except near $n \approx 25$), for Ar the corresponding oscillatory maxima first decrease and then rise sharply as n increases. The RT effect consists in a non-monotonic energy dependence of $d\sigma_{el}/d\Omega$ for low-energy electron scattering by multielectron atoms and ions due to an interplay of partial scattering amplitudes with different l. For field-free e-Ar scattering, the RT effect leads to a minimum in the DCS ("RT minimum"), whose position ($E \approx E_{\rm R}$) depends on the scattering angle θ and is in the region $E_{\rm R} \lesssim 1$ eV [for the total (angle-integrated) cross section, $E_{\rm R} \approx 0.3$ eV [29]]. Since the RT effect does not exist for e-Ne scattering, for which only the s-wave phase shift $\delta_0(E)$ dominates at small energies, the aforementioned difference between results for Ar and Ne originates from the RT effect in the DCS $d\sigma_{el}[\mathbf{P}(t_c), \mathbf{P}_n(t_c)]/d\Omega_{\mathbf{P}_n(t_c)}$ for e-Ar scattering, in which case the energy $\mathcal{E}(t_c)$ (which equals zero for $n = 0$) passes through the RT minimum with increasing n.

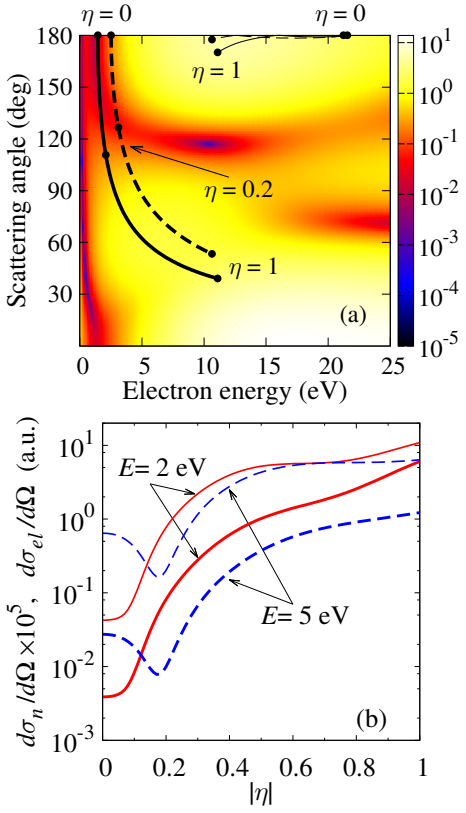

FIG. 3. (Color online) (a) The DCS $d\sigma_{el}/d\Omega$ for e-Ar scattering vs. scattering angle and electron energy. The η-dependences of the instantaneous kinetic energy $\mathcal{E}_i$ and scattering angle θ_i (see text) are shown by thick (thin) lines for the first (second) collision, $i = 1(2)$, for two incident electron energies: $E = 2$ eV (solid lines); $E = 5$ eV (dashed lines). (b) The η-dependences of the DCS $d\sigma_n/d\Omega$ for LAES from Ar for $n = n^{(\rm R)}_{\max}(\eta)$ (thick lines) and of the factor $d\sigma_{el}(\mathbf{P}, \mathbf{Q})/d\Omega_{\mathbf{Q}}$ in Eq. (8) (thin lines). For both panels, the scattering geometry and laser parameters are the same as in Fig. 1.

B. The high-energy plateau

The high-energy (rescattering) part of each LAES spectrum in Figs. 1 and 2 exhibits the effects of electron-atom dynamics even more impressively than the low-energy one. For low incident electron energy ($E = 2$ eV), the average enhancement of $d\sigma_n/d\Omega$ for e-Ar scattering over the rescattering plateau region reaches more than three orders of magnitude as η increases from $\eta = 0$ to $\eta = 1$. In contrast, the average magnitude of $d\sigma_n/d\Omega$ for e-Ne scattering does not depend on the ellipticity. As explained below, this sensitivity of $d\sigma_n/d\Omega$ to the laser ellipticity for different targets originates from dynamical features (such as the RT effect) of the DCS $d\sigma_{el}(\mathbf{P}, \mathbf{Q})/d\Omega_{\mathbf{Q}}$ in Eq. (8) that affect the η-dependence of $d\sigma_n/d\Omega$.

We analyze first the η-dependence of the kinetic energies of the electron at the first collision at time τ, $\mathcal{E}_1 = \mathbf{P}^2/(2m)$, and at the recollision event at time τ', $\mathcal{E}_2 = (\mathbf{Q}')^2/(2m)$, as well as the angles θ_1 between the instantaneous vectors $\mathbf{P}$ and $\mathbf{Q}$ and θ_2 between $\mathbf{Q}'$ and $\mathbf{P}_n$. Using the ellipticity-dependent times $\tau = \tau(\eta, \mathbf{p}, \mathbf{p}_n)$ and $\tau' = \tau'(\eta, \mathbf{p}, \mathbf{p}_n)$, we find that a linearly polarized field ($\eta = 0$) decreases the energy $\mathcal{E}_1$ (thereby facilitating return of the electron) and significantly accelerates the electron up to the rescattering event (resulting in an increased energy $\mathcal{E}_2$) [e.g., for the parameters in Fig. 1 for $E = 2$ eV, $\mathcal{E}_1 = 1.37$ eV and $\mathcal{E}_2 = 21.6$ eV]. For these collisions at $\eta = 0$, the angles θ_1 and θ_2 equal 180°, i.e., in both cases the electron backscatters from the atom. With increasing η, the energies $\mathcal{E}_1$, $\mathcal{E}_2$ tend toward each other, becoming equal ($\mathcal{E}_1 = \mathcal{E}_2 = 11.1$ eV) for circular polarization ($\eta = 1$), while the angles θ_1, θ_2 both decrease (the angle θ_1 decreases much faster than θ_2, and for $\eta = 1$, $\theta_1 = 38°$, $\theta_2 = 170°$).

Fig. 3(a) shows the DCS $d\sigma_{el}/d\Omega$ obtained using numerical results for Ar [28]. For $E = 2$ eV the thick solid line traces the curve $(\mathcal{E}_1(\eta), \theta_1(\eta))$ over the interval $0 \le \eta \le 1$, while $(\mathcal{E}_2(\eta), \theta_2(\eta))$ is given by the thin solid line. One sees that $\mathcal{E}_1$ approaches the RT minimum in the

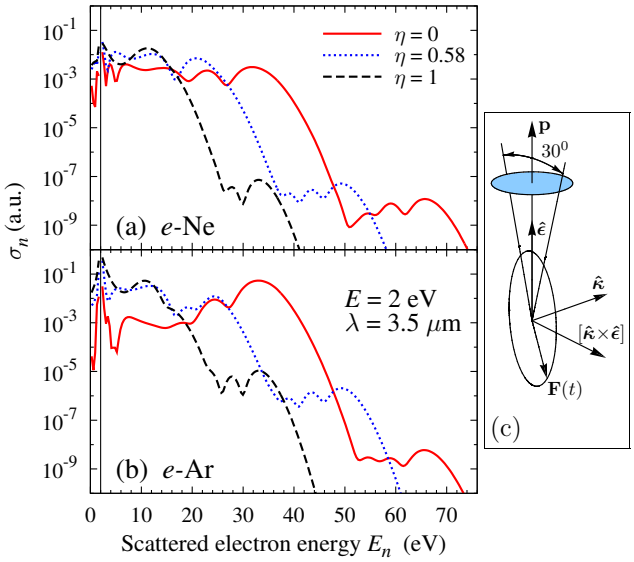

FIG. 4. (Color online) The LAES angle-integrated cross section for e-Ne and e-Ar scattering over the "forward scattering" cone with an aperture angle of 30° [cf. panel (c)] vs. scattered electron energy, $E_n = E + n\hbar\omega$. The laser field parameters and the incident electron energy E are the same as in Figs. 1 (a,b). The solid vertical lines denote $n = 0$.

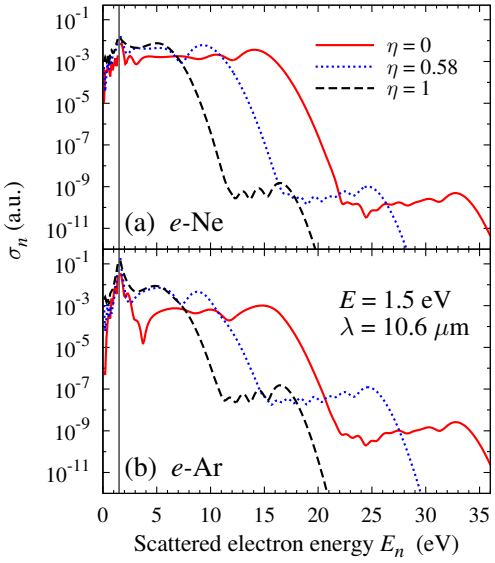

FIG. 5. (Color online) The same as in Fig. 4, but for $\hbar\omega = 0.117$ eV ($\lambda = 10.6$ μm), $I = 3.35 \times 10^{11}$ W/cm^2 ($u_p = 3.5$ eV), and $E = 1.5$ eV.

DCS as $\eta \to 0$. Thus, the suppression of $d\sigma_n/d\Omega$ for Ar for $\eta = 0$ originates from the RT effect, which does not exist in e-Ne scattering. For $E = 5$ eV the corresponding curves are given by the thick and thin dashed lines. One sees that $\mathcal{E}_1$ is outside the region of the RT minimum. Nevertheless, suppression (by two orders of magnitude) of the LAES spectrum for e-Ar scattering occurs for nonzero ellipticity [cf. Fig. 2(b) for $\eta = 0.18$]. This suppression originates from another feature of atomic dynamics: the deep minimum in the angular distribution of e-Ar scattering at $\theta \approx 120°$ [cf. Fig. 3(a)] over a broad interval of electron energies. For e-Ne scattering, such a minimum in the angular distribution of the field-free DCS appears for higher energies ($\mathcal{E}_1 \gtrsim 10$ eV). Thus this minimum does not affect the LAES spectrum in Fig. 2(a).

Fig. 3(b) shows the η-dependences of $d\sigma_{el}(\mathbf{P},\mathbf{Q})/d\Omega_{\mathbf{Q}}$ and of $d\sigma_n/d\Omega$ at the cutoff [i.e., $n = n^{(\mathrm{R})}_{\mathrm{max}}(\eta)$]. The similarity in the shapes of $d\sigma_{el}(\mathbf{P},\mathbf{Q})/d\Omega_{\mathbf{Q}}$ and $d\sigma_n/d\Omega$ in Fig. 3(b) confirms that the atomic dynamics features discussed above stem primarily from the first factor in Eq. (8) for both $E = 2$ eV and $E = 5$ eV. The third factor in Eq. (8) samples a smaller, more uniform region of the DCS [cf. the thin solid and dashed lines in Fig. 3(a)].

C. Results for the angle-integrated cross section

Numerical results for the collision time t_c [which enters the elastic scattering DCS $d\sigma_{el}/d\Omega$ in Eq. (4)] as well for times τ and τ' [which enter the first and third factors of $d\sigma^{(\mathrm{R})}_n/d\Omega_{\mathbf{p}_n}$ in Eq. (8)] show only weak dependence on the scattering angle Θ within the domain $0 < \Theta < 15°$. Thus, the integration of the LAES DCS over scattering angles within a "forward scattering" cone having an aperture angle of 30° [see Fig. 4(c)] provides angle-integrated results for LAES spectra that are qualitatively similar to those discussed above for the case of forward scattering. However, since the energy positions of the oscillatory minima and maxima of the LAES DCSs depend on Θ (cf. Ref. [22]), the angle-integrated results have much smoother oscillatory patterns, allowing manifestations of electron-atom dynamical features to appear more clearly. In Fig. 4 we present angle-integrated LAES spectra for e-Ne and e-Ar scattering for the same incident electron energy E and mid-infrared laser parameters as in Fig. 1 (a,b), while in Fig. 5 we present results for $E = 1.5$ eV and a CO_2 laser field ($\lambda = 10.6$ μm) of intensity 3.35×10^{11} W/cm^2. Clearly the manifestations of the RT effect in LAES spectra are similar for both mid-infrared and CO_2 laser fields.

D. Requirements for experimental measurements

The results shown in Figs. 1, 2, and 4 are for an experimentally-accessible, mid-infrared laser wavelength (cf., e.g., Refs. [30, 31]) and a moderate intensity ($<10^{13}$ W/cm^2) at which laser excitation or ionization of rare gas atom targets is negligible. The same is true for the results shown in Fig. 5 for a CO_2 laser field. Hence, these results may stimulate improvement of experimental techniques in order to observe laser-modified electron-atom collisions with n-photon absorption or emission. With this in mind, in what follows we discuss the experimental conditions necessary for observing these effects.

In recent experiments on LAES [32–35] the observation of n-photon absorption or emission was limited to $n = 2$ owing to the very weak LAES signal for high n. We emphasize that in order to observe higher nonlinear multiphoton effects in LAES, such as the plateau-like structures, the following criteria for choosing the laser field parameters and the values of the incident electron energy should be satisfied. On the one hand, the conditions $u_p/(\hbar\omega) \gg 1$ and $E/u_p \lesssim 1$ should be fulfilled. The first condition ensures the requirement that the laser field must be treated nonperturbatively. This condition cannot be satisfied using near-infrared lasers ($\lambda \lesssim 1$ μm) without having laser intensities that are high enough ($I \gtrsim 100$ TW/cm^2) for excitation or ionization of the target. The second condition ensures that one can observe both the low-energy and the high-energy plateaus in LAES spectra. Thus, for example, in the recent experiments of Kanya et al. [32] neither of these two conditions for observing the effects we predict are fulfilled: $u_p/(\hbar\omega) = 6.8 \times 10^{-2}$ and $E/u_p = 9.4 \times 10^3$. On the other hand, analysis of the analytic results (6) and (9) shows that over the energy interval $0.2u_p < E < u_p$ the propagation factor $W(\mathbf{p}, \mathbf{p}_n)$ decreases with increasing λ and I as $W \sim \lambda^{-4.2} I^{-c}$, where $c = 0.75$ for $\eta = 0$ and $c = 0.45$ for $|\eta| = 1$ (e.g., cf. Figs. 4 and 5). Thus, one must balance the aforementioned conditions for u_p with the scaling law for the LAES DCS as $u_p \propto I\lambda^2$ increases.

The major experimental difficulty in observing multiphoton LAES signals stems from the extremely small count rate, $\mathcal{R}$, of scattered electrons. This rate is proportional to the product of two crucial factors: the repetition rate of the data accumulation (i.e., the duty cycle, D) and the volume (V) of the overlap of the atomic, electron and laser beams. Specifically, $\mathcal{R} \backsimeq \sigma_n j_e n_a V D$, where j_e is the flux of incident electrons and n_a is the density of target atoms. The typical pulse duration Δt for currently available intense mid-infrared lasers is $\Delta t \sim 100$ fs at a repetition rate $\Omega \sim 1$ kHz [30], so that $D = \Omega\Delta t \sim 10^{-10}$, while the volume V is governed by the typical diameter (~ 0.1 mm) of the focal area for a laser field with $I \sim 10^{13}$ W/cm^2. However, Ref. [33] notes that a significant increase in the count rate of LAES signals by three orders of magnitude will be achieved in the near future owing to rapid advances in the technology of high-power and high-repetition-rate femtosecond fiber lasers (specifically, owing to increased values for D).

With regard to the results for the CO_2 laser wavelength presented in Fig 5, we note that despite the aforementioned λ-scaling of the LAES cross section, the latest developments in producing high-power (>10 GW) CO_2 laser pulses with Δt ~3 ps (cf. Refs. [36, 37]) provide another promising way to observe multiphoton effects in LAES (at least for values of n corresponding to the low-energy plateau). Such pulses (separated by 18 ps) are combined in macropulses having total durations of ~100 ps and possible repetition rates up to 1 kHz [36]. (Note that the laser intensity in past LAES experiments with pulsed CO_2 lasers was smaller than 10^9 W/cm^2; cf. Ref. [34] and references therein.) Besides having the appropriate ratio $u_p/(\hbar\omega) \gg 1$ and a higher duty cycle (up to $D \sim 10^{-8}$), the use of such powerful pulses holds the possibility of increasing the interaction volume V by orders of magnitude.

Finally, we emphasize that the count rate for the LAES signal depends crucially on the dynamical features of the field-free electron-atom interaction, which can result in pronounced variations of LAES cross sections σ_n. For the case of low-energy electron scattering on atoms of heavy rare gases assisted by linearly polarized or small-ellipticity ($\eta \lesssim 0.2$) laser fields, the LAES cross sections are significantly suppressed due to manifestations of the RT effect. As discussed above, such suppression may be eliminated by increasing the ellipticity of the laser field.

IV. CONCLUSION

In this paper, we have predicted manifestations of electron-atom dynamics in LAES using the present generalization of our recent TDER results [22] for LAES in an elliptically polarized laser field to the case of electron scattering by neutral atoms. As we have shown, the use of an elliptically polarized laser field provides a means to control the manifestation of field-free electron-atom dynamics in LAES. In particular, varying the laser ellipticity may allow the enhancement (by orders of magnitude) of LAES cross sections for target atoms having special features (such as the RT minimum) in their field-free DCS for low-energy elastic scattering. This proposed mechanism for LAES cross section enhancement should be considered when planning experiments on multiphoton LAES.

ACKNOWLEDGMENTS

We gratefully acknowledge O. Zatsarinny for providing theoretical results for elastic electron scattering from Ne and Ar. We also gratefully thank T. J. Gay for detailed discussions of techniques for experimental LAES measurements. This work was supported in part by RFBR Grant No. 13-02-00420 and by NSF Grant No. PHYS-1208059.

[1] P. Salières, B. Carré, L. Le Déroff, F. Grasbon, G. G. Paulus, H. Walther, R. Kopold, W. Becker, D. B. Milošević, A. Sanpera, and M. Lewenstein, Science **292**, 902 (2001).

[2] W. Becker, F. Grasbon, R. Kopold, D. B. Milošević, G. G. Paulus, and H. Walther, Adv. At. Mol. Opt. Phys. **48**, 35 (2002).

[3] D. B. Milošević and F. Ehlotzky, Adv. At. Mol. Opt. Phys. **49**, 373 (2003).

[4] N. L. Manakov, A. F. Starace, A. V. Flegel, and M. V. Frolov, Pis'ma Zh. Eksp. Teor. Fiz. **76**, 316 (2002) [JETP Lett. **76**, 258 (2002)].

[5] A. Čerkić and D. B. Milošević, Phys. Rev. A **70**, 053402 (2004).

[6] N. M. Kroll and K. M. Watson, Phys. Rev. A **8**, 804 (1973).

[7] K. J. Schafer, B. Yang, L. F. DiMauro, and K. C. Kulander, Phys. Rev. Lett. **70**, 1599 (1993).

[8] P. B. Corkum, Phys. Rev. Lett. **71**, 1994 (1993).

[9] T. Morishita, A.-T. Le, Z. Chen, and C. D. Lin, Phys. Rev. Lett. **100**, 013903 (2008).

[10] M. V. Frolov, N. L. Manakov, T. S. Sarantseva, M. Yu. Emelin, M. Yu. Ryabikin, and A. F. Starace, Phys. Rev. Lett. **102**, 243901 (2009).

[11] M. V. Frolov, D. V. Knyazeva, N. L. Manakov, A. M. Popov, O. V. Tikhonova, E. A. Volkova, Ming-Hui Xu, Liang-You Peng, Liang-Wen Pi, and A. F. Starace, Phys. Rev. Lett. **108**, 213002 (2012).

[12] A. D. Shiner, B. E. Schmidt, C. Trallero-Herrero, H. J. Wörner, S. Patchkovskii, P. B. Corkum, J. Kieffer, F. Légaré, and D. M. Villeneuve, Nature Phys. **7**, 464 (2011).

[13] C. I. Blaga, J. Xu, A. D. DiChiara, E. Sistrunk, K. Zhang, P. Agostini, T. Miller, L. F. DiMauro, and C. D. Lin, Nature **483**, 194 (2012).

[14] A. V. Flegel, M. V. Frolov, N. L. Manakov, and A. N. Zheltukhin, J. Phys. B **42**, 241002 (2009).

[15] T. Kanai, S. Minemoto, and H. Sakai, Phys. Rev. Lett. **98**, 053002 (2007).

[16] J. Higuet, H. Ruf, N. Thiré, R. Cireasa, E. Constant, E. Cormier, D. Descamps, E. Mével, S. Petit, B. Pons, Y. Mairesse, and B. Fabre, Phys. Rev. A **83**, 053401 (2011).

[17] D. Shafir, B. Fabre, J. Higuet, H. Soifer, M. Dagan, D. Descamps, E. Mével, S. Petit, H.J. Wörner, B. Pons, N. Dudovich, and Y. Mairesse, Phys. Rev. Lett. **108**, 203001 (2012).

[18] M. Möller, Y. Cheng, S. D. Khan, B. Zhao, K. Zhao, M. Chini, G. G. Paulus, and Z. Chang, Phys. Rev. A **86**, 011401(R) (2012).

[19] M. V. Frolov, N. L. Manakov, T. S. Sarantseva, and A. F. Starace, Phys. Rev. A **86**, 063406 (2012).

[20] A. V. Flegel, M. V. Frolov, N. L. Manakov, and A. F. Starace, Phys. Lett. A **334**, 197 (2005).

[21] A. Čerkić, M. Busuladžić, E. Hasović, A. Gazibegović-Busuladžić, S. Odžak, K. Kalajdžić, and D. B. Milošević, Phys. Scr. **T149**, 014044 (2012).

[22] A. V. Flegel, M. V. Frolov, N. L. Manakov, A. F. Starace, and A. N. Zheltukhin, Phys. Rev. A **87**, 013404 (2013).

[23] L. D. Landau and E. M. Lifshitz, *Quantum Mechanics* (Pergamon, Oxford, 1992), 4th ed.

[24] N. L. Manakov, A. F. Starace, A. V. Flegel, and M. V. Frolov, Pis'ma Zh. Eksp. Teor. Fiz. **87**, 99 (2008) [JETP Lett. **87**, 92 (2008)].

[25] D. B. Milošević, Phys. Rev. A **53**, 619 (1996).

[26] L. B. Madsen and K. Taulbjerg, J. Phys. B **31**, 4701 (1998).

[27] O. Zatsarinny and K. Bartshat, J. Phys. B **37**, 2173 (2004).

[28] O. Zatsarinny, Private communications.

[29] M. Kurokawa, M. Kitajima, K. Toyoshima, T. Kishino, T. Odagiri, H. Kato, M. Hoshino, H. Tanaka, and K. Ito, Phys. Rev. A **84**, 062717 (2011).

[30] A. D. DiChiara, E. Sistrunk, C. I. Blaga, U. B. Szafruga, P. Agostini, and L. F. DiMauro, Phys. Rev. Lett. **108**, 033002 (2012).

[31] T. Popmintchev *et al.*, Science **336**, 1287 (2012).

[32] R. Kanya, Y. Morimoto, and K. Yamanouchi, Phys. Rev. Lett. **105**, 123202 (2010).

[33] R. Kanya, Y. Morimoto, and K. Yamanouchi, Rev. Sci. Instrum. **82**, 123105 (2011).

[34] D. Nehari, J. Holmes, K. M. Dunseath, and M. Terao-Dunseath, J. Phys. B **43**, 025203 (2010).

[35] B. A. deHarak, L. Ladino, K. B. MacAdam, and N. L. S. Martin, Phys. Rev. A **83**, 022706 (2011).

[36] S. Ya. Tochitsky, J. J. Pigeon, D. J. Haberberger, C. Gong, and C. Joshi, Opt. Express **20**, 13762 (2012).

[37] D. Haberberger, S. Tochitsky, F. Fiuza, C. Gong, R. A. Fonseca, L. O. Silva, W. B. Mori, and C. Joshi, Nature Phys. **8**, 95 (2012).